Polish Journal of Microbiology
2018, Vol. 67, No 4, 417–429
https://doi.org/10.21307/pjm-2018-050

ORIGINAL PAPER

Functional and Transcriptomic Characterization of a Dye-decolorizing Fungus from *Taxus* Rhizosphere

DA CHENG HAO[1]*, SI MENG SONG[1], YAN CHENG[1], ZHI QIANG QIN[1], GUANG BO GE[2, 3], BAI LIN AN[1] and PEI GEN XIAO[4]

[1] Biotechnology Institute, School of Environment and Chemical Engineering, Dalian Jiaotong University, Dalian, China
[2] Dalian Institute of Chemical Physics, Chinese Academy of Sciences, Dalian, China
[3] Shanghai University of Traditional Chinese Medicine, Shanghai, China
[4] Institute of Medicinal Plant Development, Chinese Academy of Medical Sciences, Beijing, China

Submitted 19 April 2018, revised 23 June 2018, accepted 10 July 2018

Abstract

We isolated three laccase-producing fungus strains from *Taxus* rhizosphere. *Myrotheium verrucaria* strain DJTU-sh7 had the highest laccase activity of 216.2 U/ml, which was increased to above 300 U/ml after optimization. DJTU-sh7 had the best decolorizing effect for three classes of reactive dyes. The DJTU-sh7-containing fungal consortium displayed the robust decolorizing ability. Both color removal efficiency and chemical oxygen demand were increased in the consortium mediated biotransformation. Transcriptome changes of *M. verrucaria* elicited by azo dye and phenolic were quantified by the high throughput transcriptome sequencing, and the activities of the selected oxidases and reductases were determined. The possible involvement of oxidases and reductases, especially laccase, aryl alcohol oxidase, and ferric reductase in the biotransformation of dye and phenolic compounds was revealed at both transcriptomic and phenotypic levels. Revealing the transcriptomic mechanisms of fungi in dealing with organic pollutants facilitates the fine-tuned manipulation of strains in developing novel bioremediation and biodegradation strategies.

Key words: *Myrothecium*, reactive dye decolorization, laccase, transcriptome sequencing, degradation mechanism

Introduction

Nature mining for bioactive enzymes from plants and microorganisms is highlighted in building a sustainable bio-based economy. The typical reaction of laccase is the oxidation of a phenolic compound with the concurrent reduction of molecular oxygen to water (Schaechter 2009). Laccases have very broad substrate specificities and can oxidize a variety of substrates, such as di- and polyphenols, aromatic amines, and a considerable range of other compounds. Laccase is effective in dye decolorization (Bello-Gil et al. 2018; Hao et al. 2016), and it can be combined with other enzymes in the bioremediation of reactive dye (Khan and Fulekar 2017). Laccase has the potential to be implemented in various industrial fields, such as biomass conversion, waste water treatment (Jasińska et al. 2015), polymer syntheses, and remediation of bio-based chemicals, etc. Laccase-producing fungi have found uses in a wide range of technological applications (Chitradevi and Sivakumar 2011; Forootanfar and Faramarzi 2015). However, the great potential of rhizosphere as a gold ore of laccase-producing fungi has not been fully investigated and there is no report concerning about such strains from *Taxus* rhizosphere.

Currently synthetic dyes are used broadly in the textile dyeing, paper printing, color photography, pharmaceuticals, food and drink, cosmetic and leather industries. At present, more than 100 000 diverse dyes are present, with a yearly production of above 700 000 metric tons. These industries release a massive amount of colored effluents into natural water bodies, with or without treatment. The textile industry alone discharges 280 000 tons of dyes annually (Patel et al.

* Corresponding author: D.C. Hao, Biotechnology Institute, School of Environment and Chemical Engineering, Dalian Jiaotong University, Dalian, China; **e-mail: hao@djtu.edu.cn**

2015), making it the principal contributor to tinted effluent discharge.

Although a variety of treatment technologies are accessible, e.g., adsorption, chemical oxidation, precipitation, coagulation, filtration electrolysis and photodegradation, the biological and microbiological methods using activated sludge, pure cultures, microbial consortia and degradative enzymes are cost-effective and eco-friendly alternatives. However, little information of fungi mediated decolorization is available for most dyes. For instance, the nonviable biomass of *Rhizopus nigricans* was reported to adsorb reactive green (RG) 19 (Kumari and Abraham 2007), but whether any fungus is able to degrade it is not known. Fungi efficient for azo dyes are not necessarily suitable for anthraquinone and/or phthalocyanine dyes (Baratto et al. 2015), and *vice versa*. The fungal profile for decolorizing various dye classes has not been fully investigated. Abundant data should be gathered from more extensive studies on the fungal degradation of synthetic dyes, offering researchers and industries the latest information and the expanded reference guide on the subject.

Myrothecium verrucaria is a species of fungus in the order Hypocreales (Sordariomycetes, Ascomycota), which is distributed globally but has not been found in the *Taxus* rhizosphere. A *M. verrucaria* strain NF-05 displays its biotechnological potential in dye decolorization (Zhao et al. 2012). *Taxus* (the source plant of the anticancer taxanes) rhizosphere can contribute to prospective biotransformation strains (Hao et al. 2008; Dou et al. 2015), which inspire us to further probe the functional potential of *Taxus* rhizosphere microbiota. We hypothesize that the *M. verrucaria* strain DJTU-sh7, with the highest laccase activity, could be effective in decolorizing three classes of reactive dyes. We also hypothesize that the transcriptomic changes of DJTU-sh7 upon azo dye elicitation could at least partially explain the underlying molecular mechanisms of fungal decolorization of azo dye. In this study, we isolated laccase-producing fungus strains, including a new *M. errucaria* strain DJTU-sh7, from the rhizosphere soil of three *Taxus* species, i.e., *T. mairei* (NF), *T. cuspidata var. nana* (ZS), and *T.* × *media* (MD). The laccase production of DJTU-sh7 was optimized via single factor experiments and the uniform design. Transcriptome analysis was performed to elucidate the molecular mechanisms of Direct Red 5B azo dye degradation in white rot fungus *Irpexlacteus* CD2 (Sun et al. 2016). RNA Seq analysis was performed to study the role of calcium chloride stress and electron transport in mitochondria for malachite green decolorization by *Aspergillus niger* (Gomaa et al. 2017). These pioneering works illustrate the power of transcriptome characterization in deciphering the fungal transformation of dye pollutants. Here, the dye removal abilities of DJTU-sh7 were characterized and the transcriptomic mechanisms of azo dye decolorization and biotransformation were revealed for the first time.

Experimental

Materials and Methods

Decolorization of reactive dyes. Six azo dyes (reactive deep blue M-2GE, reactive navy blue B-GD, reactive brilliant red KE-7B, reactive brilliant orange K-GN, RG19, and reactive black 5) were purchased from Sigma Company. Two anthraquinone dyes (reactive brilliant blue K-3R and X-BR) and the phthalocyanine dye reactive turquoise blue KN-G were from Shanghai Jiaying Chemical Engineering Co., Ltd. The degradation of nine structurally different dyes by the fungal culture/crude laccase was determined by full spectrum scan among 400–700 nm between 0–96 h. The dye decolorization was calculated at various time points. The reaction mixture for the standard assay contained respective dye (20 mg/l) in 10 mM citric acid-Na_2HPO_4 buffer at pH 4.5 and 1 ml of fungal suspension/crude laccase in a total volume of 10 ml. The dye decolorization (%) = $[(A_i - A_t)/A_i] \times 100$, where A_i – initial absorbance of the dye, A_t – absorbance of the dye along the time. All experiments were performed in triplicate. The maximal absorbance wavelength of these dyes is 612 nm (reactive deep blue), 596 nm (reactive navy blue), 565 nm (reactive brilliant red), 479 nm (reactive brilliant orange), 632 nm (RG19), 597 nm (reactive black), 623 nm (reactive brilliant blue K-3R), 596 nm (X-BR) and 601 nm (reactive turquoise blue), respectively.

One ml of RG19 at a concentration of 20–500 mg/l was mixed with 0.5 ml of each fungal suspension (two member consortium) or 0.333 ml of each fungal suspension (three member consortium) and 8 ml H_2O. Thus, the final concentration of RG19 was 2–50 mg/l. Each experiment was performed in triplicate at 30°C for 4 days, and the dye decolorization was determined as described above. Different reactive dyes, mixed with the equal ratio, were used in the dye decolorization. COD was determined by the standard potassium dichromate method.

Chromatography and spectroscopy. The degradation mixture was centrifuged, and pH of the supernatant was adjusted to 5.0. Extraction of products from the supernatant was performed using equal volume of chloroform, and the extract was then evaporated in vacuum and dried. The solid residue obtained was dissolved in 1 ml chloroform and 1 ml methanol for thin layer chromatography (TLC), and the 365 nm UV light was used to observe TLC results.

For high performance liquid chromatography (HPLC), the above solid residue was dissolved in

a small volume of HPLC-grade methanol, and the sample was then used for analytical studies. This was the test sample. A dye solution of 20 mg/l was used as a biotic control. Agilent1200 (Palo Alto, CA) HPLC conditions: C18 column, 250 × 4.6 × 5 μm, 30°C, injection volume 5 μl, flow speed 1 ml/min, mobile phase H_2O/acetonitrile, detection wavelength 632 nm. Gradient elution: 0–15 min, H_2O 90%/acetonitrile 10%; 15–21 min, H_2O 10%/acetonitrile 90%; 21–25 min, H_2O 90%/acetonitrile 10%.

The biotransformation was monitored using FTIR (Fourier transform infrared) (Bio-Rad FTIR Model FTS 135) and compared with the control sample. The FTIR analysis was performed in the mid-IR region of 450–4000 cm^{-1} with 16 scan speed. C18 solid phase microextraction column (Agilent) was used to extract degradation products from the filtered supernatant, with dichloromethane as the elution solvent and the elution rate 2 ml/min. The samples were mixed with spectroscopically pure KBr in the ratio of 5:95, pellets were fixed in the sample holder, and the IR scan was performed. The dye decolorization was monitored via UV-Vis spectroscopic analysis (Hitachi U-2800, Japan), using supernatants.

RNA extraction. The single colonies of *M. verrucaria* were inoculated into three 500 ml flasks of the following medium: sucrose 2 g, peptone 1 g, KH_2PO_4 0.2 g, $MgSO_4$ 0.05 g, $CaCl_2$ 0.0075 g, $CuSO_4$ 0.001 g, H_2O to 100 ml, which was control culture without guaiacol or RG19 (named "ordi"). The single colonies from the same culture plate were also inoculated into three 500 ml flasks of the ordinary medium supplemented with 0.04% guaiacol (named "guai"). Similarly, the single colony was grown in the ordinary medium supplemented with 5 mg/l RG19 (named "green"). After 5-d shaking flask culture at 25°C, the fresh medium with the same components as the initial medium of each group was added into the respective flask. The fungal mycelia of the same group were collected and mixed together for RNA extraction after another 24 h culture. Total RNA was extracted from *M. verrucaria* using the TRIzol reagent. RNA integrity was checked on a 1% agarose gel. The total RNA from three technical replicates of ordi was mixed equally, and the RNA mixture was obtained from guai and green respectively. RNA concentrations were determined using a NanoDrop 2000C spectrophotometer (Thermo Scientific, USA). RNA with OD260/280 = 1.8–2.2 and OD260/230 = 1.8 was used in the transcriptome sequencing.

Transcriptome sequencing and bioinformatics analysis. The transcriptome sequencing libraries of ordi, guai and green were constructed as previously described (Hao et al. 2015). The library products were sequenced via Illumina HiSeq 4000 sequencer. By base calling, the original image data for three groups (control, guaiacol and RG19 treatments) produced by the sequencer was transferred into raw reads, available at NCBI Sequence Read Archive (accession nos. SRR5738138, SRR5738139, and SRR5738140). After data cleaning, Trinity (http://trinityrnaseq.sourceforge.net/) was used in the de novo sequence assembly. Clean reads (ordi 30 334 130, guai 30 229 428, and green 29 541 586) were mapped to the assembled Unigenes, using Bowtie 2 (http://bowtie-bio.sourceforge.net/bowtie2/index.shtml), for analysis of differentially expressed genes (DEGs). Unigene expression levels are presented in FPKM (Fragments Per Kb of exon per Million fragments mapped).

The functional annotations were performed by the alignments with NCBI Nt, NR, SwissProt, KOG and KEGG databases using Blast N (Nt) or Blast X/Diamond (the rest) (Buchfink et al. 2015). BLAST2GO (default parameters; http://www.blast2go.com/) and the GO database (http://www.geneontology.org) were used for the functional annotation of biological process, molecular function and cellular component. InterProScan 5 (http://www.ebi.ac.uk/interpro/search/sequence-search) was used for the InterPro annotation. Trinity and Transdecoder (https://help.rc.ufl.edu/doc/TransDecoder) were used to predict the open reading frame (ORF) and protein-coding sequence (CDS).

The software RSEM (http://deweylab.biostat.wisc.edu/rsem/) was used to calculate the gene expression level from RNA-Seq data. FDR (false discovery rate) ≤ 0.001 and the absolute value of $\log_2$fold change ≥ 1 were used as the threshold to judge the significance of gene expression difference (Hao et al. 2011). Cluster analysis of expression patterns of 21 220 Unigenes, expressed in all three conditions (ordi, guai, and green), was performed with software Mfuzz (Kumar and E Futschik 2007). The pheatmap function of R package (https://www.r-project.org/) was used to perform the hierarchical cluster analysis for DEGs.

The GO classification and KEGG pathway visualization of DEGs were performed. The pathway enrichment analysis by the phyper function of R package identified significantly enriched metabolic pathways and signal transduction pathways in DEGs compared with the reference gene background. The Q value was obtained by the Bonferroni correction of the p value. Pathways with q values ≤ 0.05 are significantly enriched in DEGs.

Proteins usually perform functions after they are combined into a complex by interaction. The interacting DEGs usually have similar functions. In this study, DEGs were mapped to STRING database (https://string-db.org/), and the homology between the known protein and DEG encoding protein was utilized to obtain the interaction relationship between DEG encoding proteins.

Quantifying activities of oxidase and reductase. The reaction mixture of 10 ml consisted of 0.04 mmol guaiacol (Sheikhi et al. 2012; Zhao et al. 2012) in 1 ml 95% ethanol, 1 ml crude enzyme, and 8 ml sodium succinate buffer, which reacted for 30 min at 30°C and were subjected to absorbance determination at 465 nm. The inactivated crude enzyme (boil for 5 min) was used as the negative control. One unit of the laccase activity was defined as the enzyme amount that was used to catalyze the oxidation of 1 nmol guaiacol within 1 min. In laccase activity (U/ml) = $10^6 \times$ reaction volume $\times \Delta A$ / (volume of crude enzyme $\times$ absorbance coefficient $\varepsilon \times \Delta t$), ΔA is the change of absorbance and Δt is the reaction time.

Cells of pure *M. verrucaria* strains grown in culture medium containing 20 mg/l RG19 for 72 h or 96 h were collected by centrifugation (5000 × g for 20 min). The supernatant after centrifugation was used for determining the activities of extracellular enzymes. The cell pellet was washed for three times with 10 mM potassium phosphate buffer (pH 7.2) to eliminate the influence of potential extracellular enzyme on quantifying the intracellular enzyme activity. The supernatant of the ultrasonicated cell suspension was used for determining the activities of intracellular enzymes.

Enzyme activities were monitored spectrophotometrically (Shanghai Metash Instruments Co., Ltd., China) with a total volume of 10 ml at room temperature (25°C). For all enzymes, the supernatant and cell suspension were boiled for 20 min and used as the control inactivated enzyme. Laccase activity was determined as described above, except that the minimal amount of carbon and nitrogen sources were used in the liquid culture. Lignin peroxidase (LiP) reaction mixture in 50 mM sodium tartrate buffer (pH 3.0) contained 10 mM veratryl alcohol as substrate, 4 mM H_2O_2 and 1.0 ml enzyme. The reaction was monitored by measuring the change at 310 nm (Jasińska et al. 2015). Manganese peroxidase (MnP) reaction mixture in 50 mM sodium malonate buffer solution (pH 4.5) contained 20 mM DMP (2,6-dimethoxyphenol) as substrate, 20 mM MnSO4, 4 mM H_2O_2 and 1.0 ml enzyme. The reaction was monitored by measuring the change at 470 nm (Jasińska et al. 2015). Tyrosinase activity was determined by the formation of *o*-benzoquinone and dehydroascorbic acid in 10 ml reaction mixture containing 50 mM of catechol, 2.1 mM of ascorbic acid and 1.0 ml enzyme in 50 mM potassium phosphate buffer (pH 6.5) and decrease in optical density (OD) was measured at 265 nm (Waghmode et al. 2011). All enzyme assays were carried at room temperature where reference blanks that contained inactivated enzyme were run along the test. Aryl alcohol oxidase (AAO) activity was determined by the formation of aryl aldehyde in 5.0 ml reaction mixture containing 10 mM *p*-anisyl alcohol (4-methoxybenzyl alcohol) (Ferreira et al. 2005) and 1.0 ml enzyme in 100 mM phosphate buffer (pH 6.0) and OD was measured at 285 nm.

NADH-dichlorophenolindophenol (DCIP) reductase activity was determined as described by Dawkar et al. (2010). The reaction mixture in 50 mM phosphate buffer solution (pH 7.4) contained 1.72 mM DCIP (2,6-dichloroindophenol sodium salt) and 0.70 mM NADH as the substrate, and 1.0 ml enzyme. The reaction was monitored by measuring the change at 620 nm. Azo reductase activity was determined according to the method described by Ramalho et al. (2005), which monitored the change of methyl orange concentration at 461 nm. Ferric reductase activity was determined according to the method described by Ramalho et al. (2005), and the absorbance at 562 nm was measured against a blank prepared similarly but with inactivated enzyme. All determinations were performed in triplicate.

Results and Discussion

Fungal strains and single factor experiments. Three laccase-producing fungal strains were isolated from the enrichment culture (Hao et al. 2016), i.e., a *Myrothecium verrucaria* (Sordariomycetes, Ascomycota) strain DJTU-sh7 from MD, a *Glomerella* (Sordariomycetes) strain from ZS, and a *Talaromyces stollii* (Eurotiomycetes, Ascomycota) strain from NF. The time course of laccase production in DJTU-sh7 was compared with those of other three laccase-producing fungi (Fig. 1). At the beginning, the mycelia grew slowly, and mycelial pellets were small with the low laccase activity in all strains. Then the mycelia grew fast and mycelial pellets became more compact and larger, while the fermentation media were clear and sticky. DJTU-sh7 displayed the highest laccase activity on day 6 (Fig. 1A), followed by the *Glomerella* strain on day 5, the *Aspergillus* strain (isolated from *Cordyceps sinensis* rhizosphere, unpublished) on day 6, and the *T. stollii* strain on day 7. The maximal mycelia dry weight came two days later than the laccase peak in DJTU-sh7 (Fig. 1B).

The process parameters that influence laccase production were optimized. The type of the carbon/nitrogen source influenced the laccase production by all strains (Fig. 1). When the carbon source was sucrose, all four strains showed the relatively higher laccase activity (Fig. 1C); when the carbon source was starch, lactose, or glucose, only DJTU-sh7 exhibited the high laccase activity; when fructose was the sole carbon source, the laccase production was meager in all strains. On the other hand, peptone could be the best nitrogen source of four strains (Fig. 1D), followed by yeast extract and beef extract, while the other four nitrogen sources were not ideal.

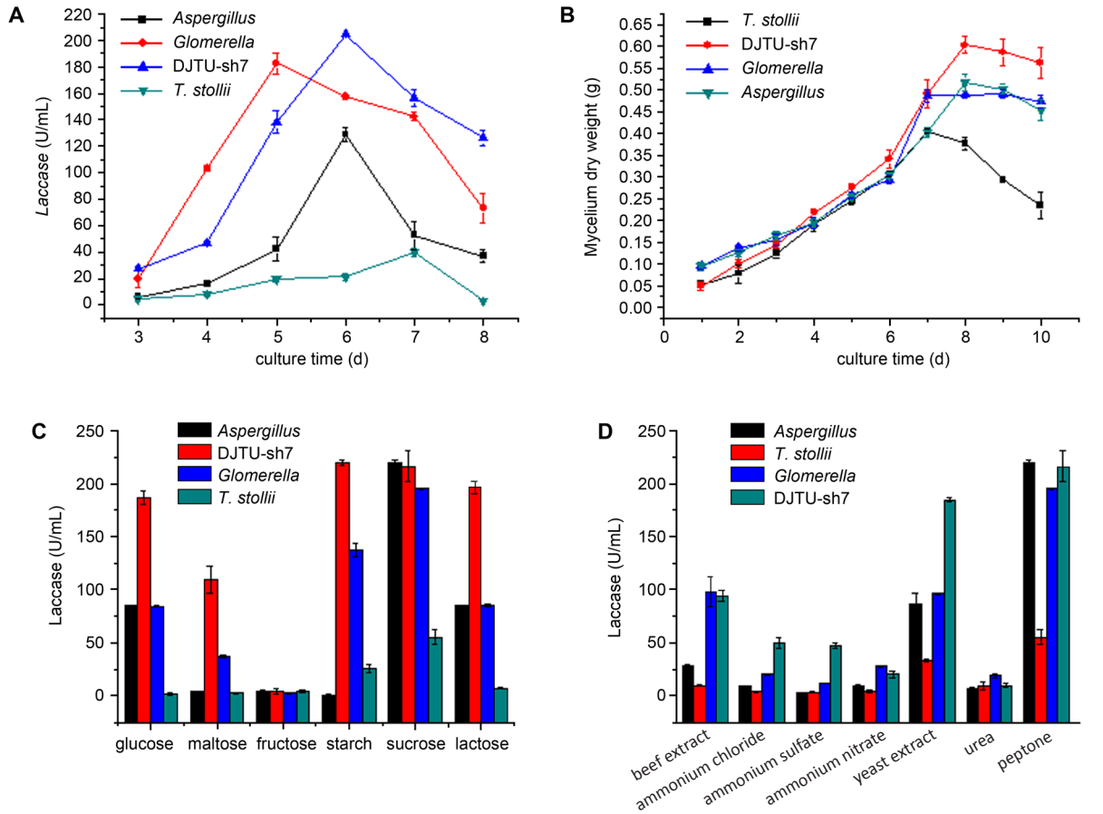

Fig. 1. A. Time course of the laccase production in four fungal strains. B. Biomass production, represented by the mycelium dry weight, of fungal strains. The 70 ml culture media contained 20 g/l glucose, 5 g/l peptone, and 5% fungal inoculant. Effects of carbon sources (C)/nitrogen sources (D) on the laccase production of four fungal strains. The agitation rate and the incubation temperature were 120 rpm and 28°C respectively.

The impacts of the incubation temperature, the initial pH, and dye concentration on the decolorization ability of DJTU-sh7 were investigated. Without fungi, adjusting pH alone did not decolorize any of the nine reactive dyes (data not shown). The maximal decolorization of 20 mg/l RG19 by the DJTU-sh7 suspension was obtained at pH 4.5 after 4 d reaction, and RG19 was decolorized within a broad range of pH 3.5–7. The maximal removal of RG19 was obtained at 35°C and pH 4.5 after 24 h shake flask culture. The conspicuous elimination of RG19 of 2–20 mg/l was observed at 35°C and pH 4.5 after 4 d reaction. The decreased decolorization of RG19 of 40–50 mg/l was obvious, implying the saturation effect of the decolorization process.

Dye decolorization. The whole cell biotransformation approach and the crude laccase were used to compare the dye decolorization performance of four fungal strains (Fig. S1A-I; also see Fig. 6 of Hao et al. 2016). The performance of the crude laccase (culture media and extracellular enzyme) of DJTU-sh7 was a little inferior to that of the DJTU-sh7 suspension culture (fungi, culture media and extracellular enzyme), but in most cases the difference between two approaches was less than 20%, implying that the dye biosorption of fungi and the intracellular factors were of minor role and the extracellular enzymes released from fungi played a major role in dye degradation and decolorization. Besides, the purified laccase of *M. verrucaria* NF-05 could decolorize a few other azo and anthraquinone dyes (Zhao et al. 2012).

A *M. verrucaria*-containing four-member fungal consortium was able to decolorize the azo dye cibacron yellow S-3R more efficiently than the individual fungus (Chitradevi and Sivakumar 2011). In this study, the dye-reducing fungal consortia were used to improve the decolorizing process of other dyes (Fig. 2A). The two-member consortium that consisted of DJTU-sh7 and *Glomerella* showed higher decolorizing efficiency than the individual strains at 40–50 mg/l RG19, implying the synergistic interaction between strains, while DJTU-sh7 alone was more efficient than both DJTU-sh7 and *Glomerella* at 2–10 mg/l RG19. On the contrary, *Aspergillus* and *T. stollii* was not significantly better than *Aspergillus* alone at most RG19 concentration values, and the consortium's performance at 50 mg/l substrate was much worse than that of either

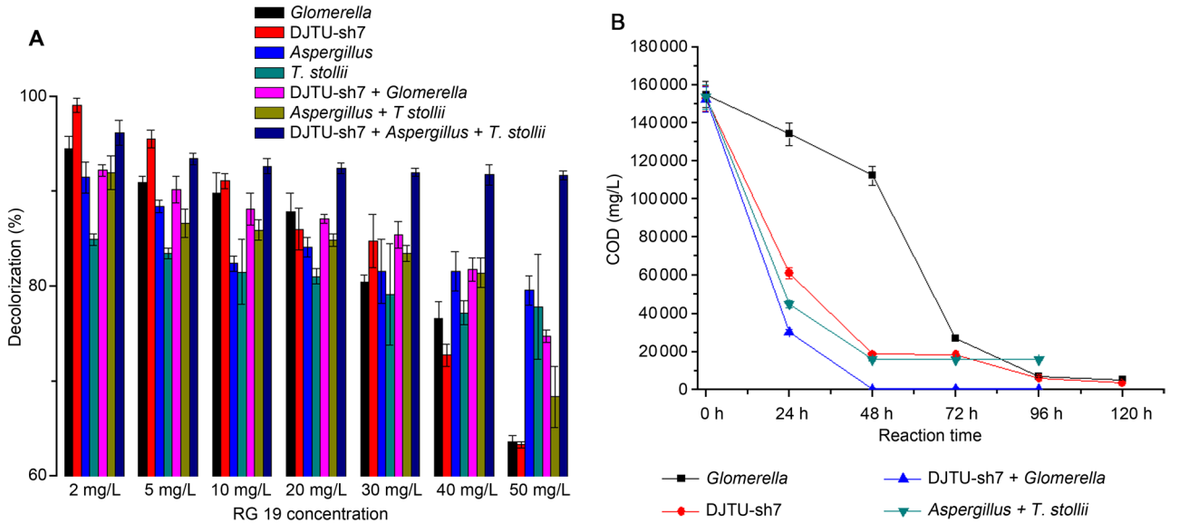

Fig. 2. A. RG19 (20 mg/l) decolorization by dye-reducing fungal consortia. B. COD removal by the fungal consortium or the single strain. The mixture of reactive dyes consists of RG19, reactive brilliant blue K-3R and X-BR (each in 6.67 mg/l). Error bars are standard deviations (n = 3).

Aspergillus or *T. stollii*, indicating the interspecific antagonistic interaction. Interestingly, the three-member consortium DJTU-sh7, *Aspergillus* and *T. stollii* displayed the robust decolorizing ability throughout various substrate concentrations, suggesting that these strains interact to achieve better dye decolorization. These results provide more diverse dye removal methods and selectivity, with research and development potential.

Three reactive dyes were mixed together, which simulated the industrial dye manufacturing effluent. COD was used to evaluate the mixed dye removal efficiency (Fig. 2B). Both color and COD removal efficiency was increased in the consortium mediated biotransformation, when compared with the single strain. The DJTU-sh7-containing consortium was more efficient than the one without it, and the initial COD value that could be processed by it is two orders of magnitude higher than that processed by a laccase-producing bacterial consortium for the treatment of industrial dye effluent (Patel et al. 2015).

Spectroscopy and chromatography. A 24-h culture of *M. verrucaria* strain DJTU-sh7 in the logarithmic phase of growth was used for the comparison studies. The UV-visible scan (400–800 nm) of medium supernatants withdrawn after 72 h of exposure to the fungi indicated decolorization and decrease in the concentration of RG19 (Fig. S2). The maximal absorbance of the decolorizing product might not fall within the range of measurements, suggesting that the dye structure was altered significantly.

The FTIR spectra before and after dye removal were compared. Peaks at 722 cm^{-1} (alkene, OH bending), 1014 and 1193 cm^{-1} (sulfonic acid group), and 1622 cm^{-1} (C-NH_2) were absent after dye decolorization, suggesting the cleavage of the azo bond and the dye degradation, which was supported by the appearance of new peaks. In TLC, a few solvent systems containing 5% acetic acid were used. In all cases, an unambiguous bright blue spot, representing the decolorizing product, was observed in the organic extract of the reaction solution under UV light, while RG 19 was significantly reduced. RG19 is a naphthol type azo dye with the hydroxyl group at *ortho* to azo bond and the electron-releasing group (i.e., -NH-triazine) (Hsueh et al. 2009). The aromatic amine is commonly found in the organic extract of the azo dye decolorization (Khandare et al. 2012). Both the azo dye and its decolorizing product are highly polar and water-soluble, which was confirmed by HPLC results. The retention time of RG19 was 1.673 min, while after transformation three putative product peaks appeared at 1.338, 1.955, and 2.134 min, respectively.

Transcriptome sequencing. RNA from *M. Verrucaria* control samples and ones undergoing guaiacol and RG19 treatments was subjected to the Illumina HiSeq4000 paired-end sequencing, which generated 30 334 130 (ordi), 30 229 428 (guai), and 29 541 586 (green) clean reads with a total of 13.51 Gb. Trinity assembled 25 415 Unigenes (ordi 17 972, guai 21 232 and green 19 059; sequences available upon request), corresponding to 31.82 Mb. The average length of the Unigenes is 1252 bp, with N50 2333 bp and GC 54.45%. A total of 20 541 Unigenes (80.82%) have at least one annotation from one the following databases. NR, Swissprot, GO, KOG, KEGG, NT, and Interpro annotations were applicable for 75.6%, 46.4%, 42.6%, 45.6%, 51.0%,

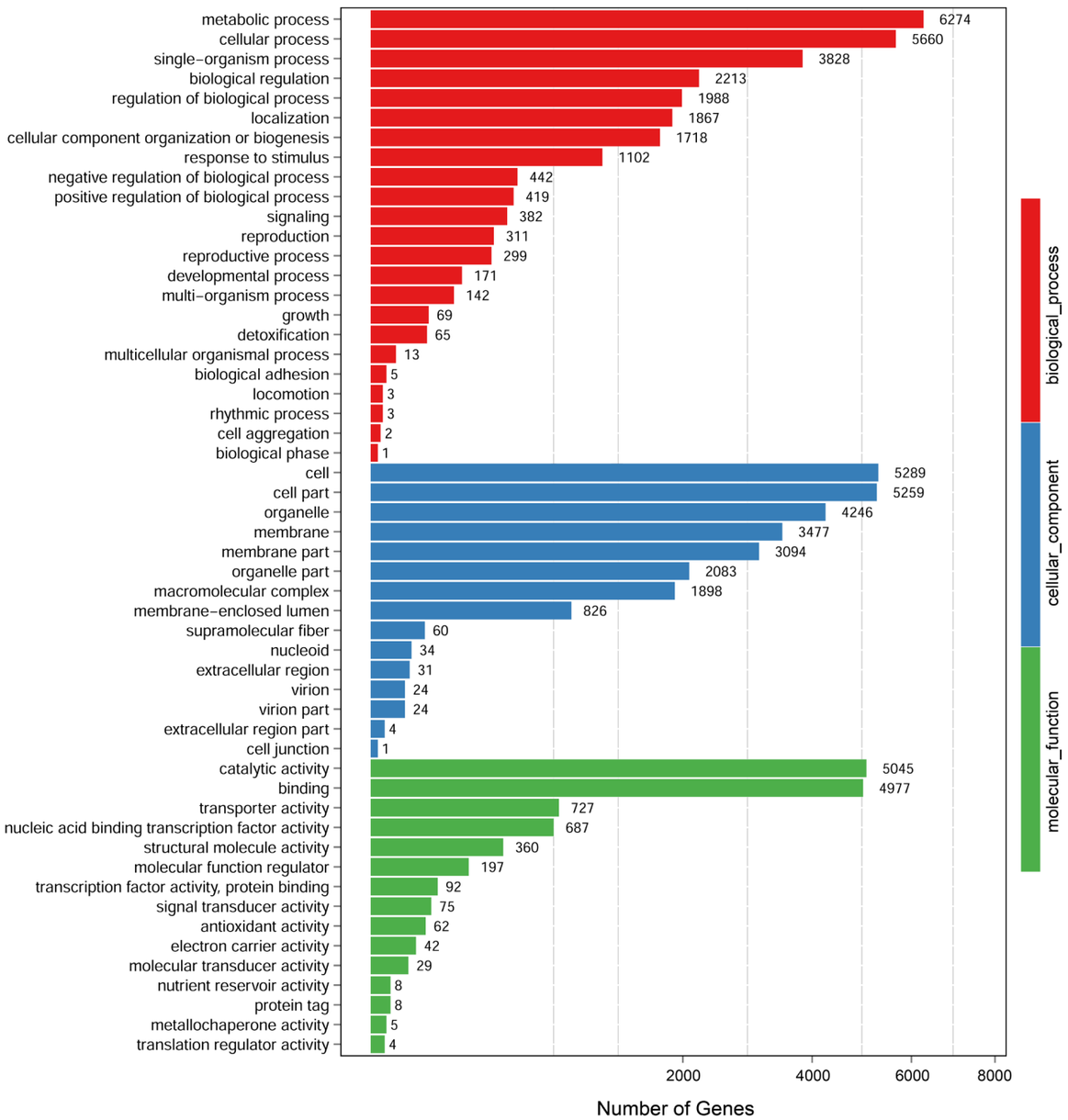

Fig. 3. A. GO annotation of biological process, cellular component and molecular function.

60.0%, and 52.7% of Unigenes, respectively. A total of 19 804 CDSs were predicted, which range between 297 and 14 538 bp, with N50 1479 bp and GC 56.0%.

In GO annotation of biological process, 6274 Unigenes belong to "metabolic process" (Fig. 3A), followed by "detoxification" (65), etc. In molecular function, 5045 Unigenes fall into "catalytic activity" (Fig. 4A), followed by "transporter activity" (727), "nucleic acid binding transcription factor (TF) activity" (687), and "antioxidant activity" (62), etc. These data indicate the great potential of *M. verrucaria* in xenobiotic metabolism and disposition. Many Unigenes involving in the biotransformation of azo dye and phenolics belong to the above GO terms. In KOG (Eukaryotic Orthologous Group) annotation, 436 and 1128 Unigenes belong to "secondary metabolite biosynthesis, transport and catabolism" and "defense mechanisms", respectively.

In KEGG annotation, 1342 (10.34% of annotated genes) belong to "Biosynthesis of secondary metabolites" and 20 belong to "Xenobiotics biodegradation and metabolism". Fifty two Unigenes belong to "Mismatch repair", followed by "Base excision repair" (52). One hundred twenty eight (0.99%) Unigenes fall into "ABC transporters". These statistics further suggest potential

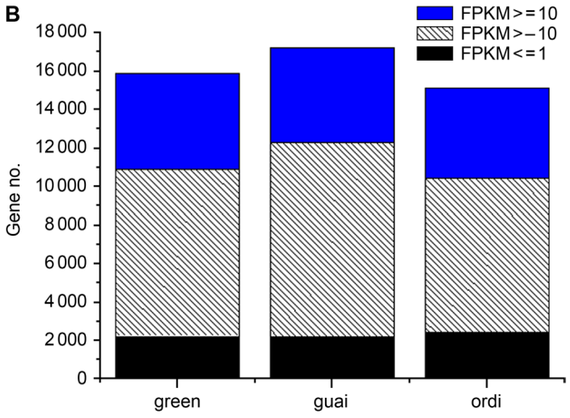

Fig. 3. B. Distribution of Unigene expression levels.

of our *Myrothecium* strain in azo dye and phenolic biotransformation.

In the control sample, 89.3% of clean reads were mapped onto the de novo-assembled Unigenes, while 88.2% and 86.6% of reads were mapped to the Unigenes in guai and green, respectively. In total, 15 123, 17 171, and 15 884 Unigenes were expressed in ordi, guai, and green, respectively, indicating that organic compound treatments induced extensive elicitor-specific transcriptome remodeling. The most abundant Unigenes in the three conditions were distinct. These results indicate dramatic transcriptome remodeling and reprogramming in *M. verrucaria* following azo dye treatment. According to the Unigene expression level distribution (Fig. 3B), in three conditions more Unigenes had the expression level between FPKM 1 and 10, followed by FPKM ≥ 10 and ≤ 1. The overlapping peaks of three conditions around $\log_{10}$FPKM 0.5 suggest that 5 mg/l RG19 was not highly toxic to the fungal strain.

Cluster analysis of expression patterns of 21 220 shared Unigenes among all three conditions (ordi, guai, and green) was performed with software Mfuzz. These genes were divided into 12 clusters. In clusters 3 (1310 Unigenes), 5 (2988), 8 (1042) and 12 (1240), the gene expression level in green was higher than those in ordi and guai. Most differentially expressed genes (DEGs) involved in azo dye biotransformation and degradation are included in these clusters and are highlighted in the following analyses.

DEGs. A total of 3586, 2159 and 3796 Unigenes had statistically significant expression differences between ordi and guai, ordi and green, and guai and green, respectively (Fig. 3C). In total 623, 445 and 674 Unigenes showed significantly different expression only between ordi and guai, ordi and green, and guai and green, respectively (Fig. 3D), but not in other two comparisons. For the DEGs, $\log_2$FC of ordi expression vs. guai expression ranged from –12.0 to 14.5. Log_2FC values of ordi vs. green and guai vs. green varied from – 11.0 to 11.7 and –14.5 to 12.7, respectively. It seems that 0.04% guaiacol elicited stronger and more

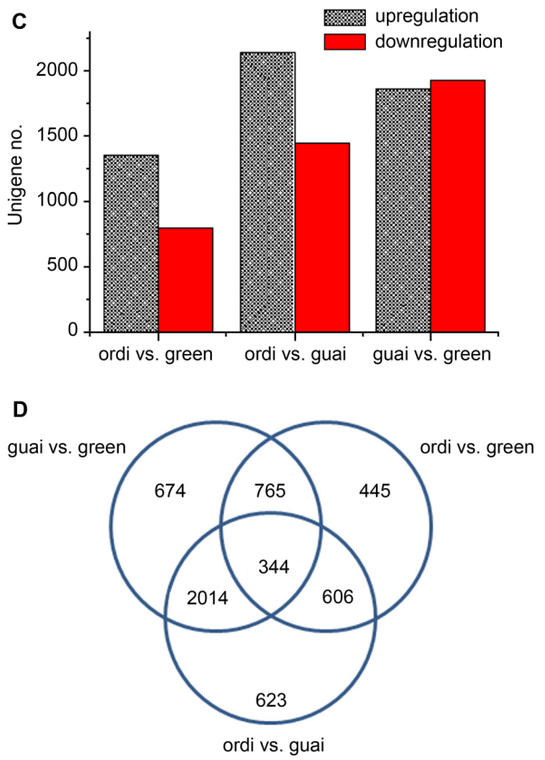

Fig. 3. C. No. of DEGs in three comparisons. In a pairwise comparison, the former one is the control and the latter the treatment. D. Common and unique DEGs of three comparisons.

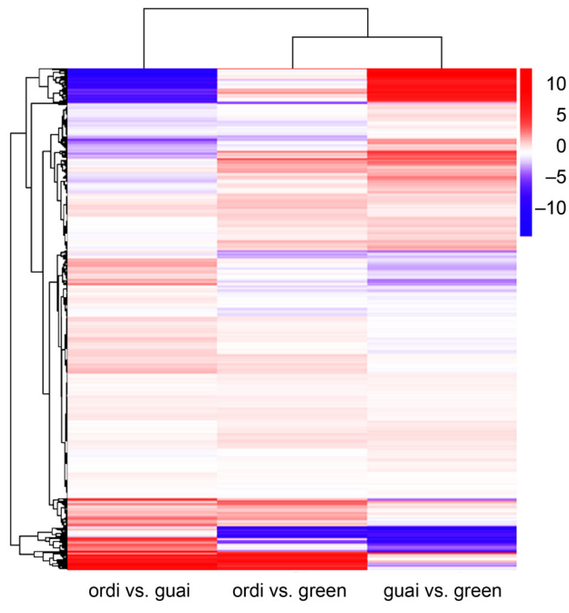

Fig. 4. Hierarchical cluster analysis of DEG union set of ordi vs. green, ordi vs. guai, and guai vs. green. The redder the color, the greater the upregulation of the gene expression; the bluer the color, the greater the downregulation of the gene expression.

extensive responses in the gene expression of *M. verrucaria* than 5 mg/l RG19.

Genes with similar expression patterns usually have the functional correlation. In the cluster analysis, 9795 DEGs fall into scores of unique clusters showing distinct expression patterns in the union set of ordi vs. guai, ordi vs. green, and guai vs. green (Fig. 4). Some clusters were identified, in which most Unigenes were upregulated in green when compared with ordi, and either upregulated, downregulated, or unaltered in guai as compared with ordi. These clusters might contain genes closely associated with dye biotransformation and decolorization. Many genes in these clusters are also involved in stress and defense responses.

The initial step of azo dye metabolism in many filamentous fungi involves the action of laccase (multicopper oxidase) and peroxidases (Fig. 5) (Solis et al. 2012; Jasińska et al. 2015). Iron transport multicopper oxidase fio1 (Unigene4094_All) was included in an 86-gene cluster and was significantly upregulated in green as compared with guai and ordi. Catalase and peroxidases are evolutionarily closely related. At least five Unigenes, representing catalase/peroxidase, had significantly higher expression in green than in other two conditions, as an essential response to oxidative stress triggered by RG19.

Monooxygenases, such as cytochrome p450 (CYP) and flavin-containing monooxygenase (FMO) are well known phase I xenobiotic metabolizing enzymes (Hao and Xiao 2011; Ma et al. 2017). At least 22 monooxygenase genes, e.g., benzoate 4-monooxygenase (five Unigenes), phenol 2-monooxygenase (four Unigenes), and dimethylaniline monooxygenase (three Unigenes), were upregulated significantly in green. For FAD-dependent monooxygenase (Unigene3165_All), the $\log_2$FC values in ordi vs. guai, ordi vs. green, and guai vs. green were

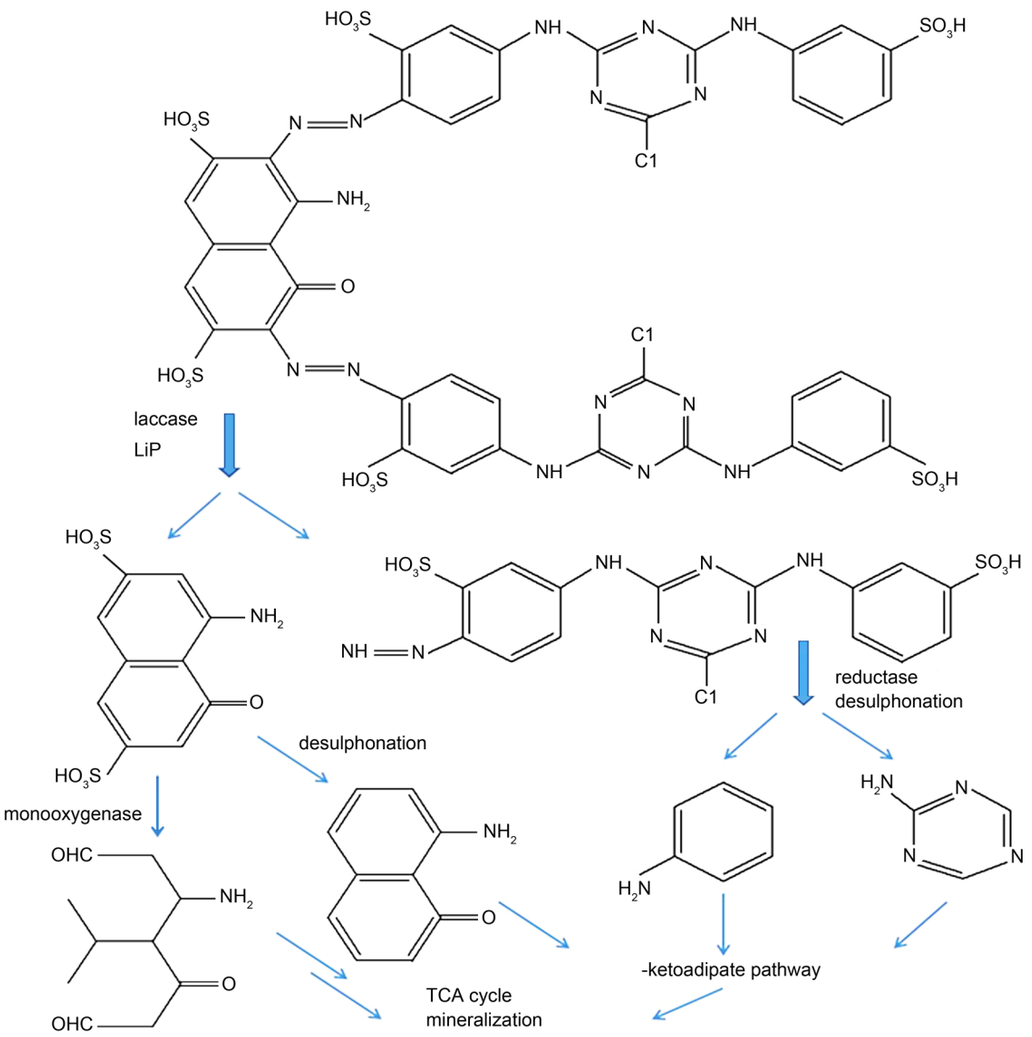

Fig. 5. Proposed degradation pathway of RG19 in *M. verrucaria*.

1.68, 3.05, and 1.38 respectively; for FMO (dimethylaniline monooxygenase CL1649.Contig2_All), the corresponding values were –0.93, 1.15, and 2.08 respectively. Alkane sulfonate monooxygenase (EC 1.14.14.5; Unigene302_All) catalyzes the transformation of alkane sulfonate ($R\text{-}CH_2\text{-}SO_3H$) + $FMNH_2$ + O_2 into aldehyde (R-CHO) + FMN + sulfite + H_2O (Zhan et al. 2008), and thus might be indispensable in azo dye desulfonation. The $\log_2$FC values of this gene in ordi vs. guai, ordi vs. green, and guai vs. green were 0.69, 1.16, and 0.47 respectively.

Phenylacetate 2-hydroxylase catalyzes the first step of phenylacetate catabolism (Rodríguez-Sáiz et al. 2001), which generates fumarate and acetoacetate and bridges between azo dye degradation intermediate and TCA cycle. Five Unigenes of this CYP were significantly increased in green. Salicylate hydroxylase [EC:1.14.13.1], catalyzing the transformation of salicylate + NADH + $2H^+$ + O_2 into catechol + NAD^+ + H_2O + CO_2, might be essential in the complete degradation of both azo dye and phenolic, as three Unigenes of this monooxygenase were significantly upregulated in both green and guai. Epoxide hydrolase (Unigene8943_All), exerting its function following CYP, was upregulated only in green. These enzymes might participate in the conversion of azo dye degradation intermediates.

Induction of the activity of aerobic enzyme dioxygenase indicates its involvement in dye removal (Cirik et al. 2013; Nor et al. 2015). Aromatic-ring-hydroxylating dioxygenases (ARHD) incorporate O_2 into their substrates in the dihydroxylation reaction. The product is (substituted) cis-1,2-dihydroxycyclohexadiene, which is subsequently converted to (substituted) benzene glycol by a cis-diol dehydrogenase, followed by ring opening. The substantially increased expression of ARHD (Unigene3184), dioxygenases (CL864.Contig1_All and Unigene3045), and isomerase (Unigene2274) suggests their prominent role in the *Myrothecium* degradation of azo dye. Our transcriptome evidence support that *Myrothecium* is able to use the β-ketoadipate pathway in degrading dye related aromatic compounds (Kim et al. 2007).

Except CYP and peroxidase, other enzymes involved in the oxidative reactions were also increased at the mRNA level. For example, tyrosinase-encoding Unigene2982_All was significantly upregulated in green ($\log_2$FC 1.81 in ordi vs. green) rather than in guai ($\log_2$FC 0.6 in ordi vs. guai) or ordi. AAO encoding Unigene7311_All had much more mRNA expression in green ($\log_2$FC 6.08 in ordi vs. green) than in guai ($\log_2$FC –1.51 in ordi vs. guai) or ordi. This enzyme was also involved in the decolorization of azo dye in *Pleurotus eryngii* (Akpinar and Urek 2014) and *Thanatephorus cucumeris* (Shimokawa et al. 2008). In contrast, the expression of MnP encoding Unigene6659_All was highest in ordi (FPKM 12.36), followed by green (6.36) and guai (2.76). Aromatic amines are metabolic intermediates during azo dye degradation (Sun et al. 2017). Copper amine oxidases (CAOs) are responsible for the oxidative deamination of aromatic amines to their corresponding aldehydes (Klema et al. 2013). The expression of CAO encoding Unigene2105_All was significantly increased in guai (FPKM 11.36) and green (1.82) as compared with ordi (0.27).

The role of reductase in the dye decolorization cannot be neglected (Song et al. 2017), especially when the oxygen supply is not sufficient. Ferric reductase-encoding Unigene558_All and Unigene7872_All were dramatically upregulated in green ($\log_2$FC1.79 and 1.2 respectively in ordi vs. green) instead of guai. In two bacterial strains, supplementation of 5 mM ferric chloride increased azo dye decolorization rate (Ng et al. 2014); ferric reductase activity was consistent with synergistic effects of ferric chloride and ferric citrate on these strains. Ferric reductase is membrane associated and involved in respiratory electron transport (Xu et al. 2007). Azo reduction by bacterial strains is coupled to the oxidation of electron donors and linked to the electron transport and energy conservation in the cell membrane (Hong and Gu 2010). Our transcriptomic and phenotypic (see below) results represent the first example of the role of ferric reductase in fungal degradation of azo dye. On the other hand, the enhanced cellular oxidation against the azo dye attack could be balanced by the upregulation of ferric reductase, which might protect cell wall integrity and mitochondrial function (Yu et al. 2014), and improve the oxidative stress tolerance (Xu et al. 2014). Correspondingly, manganese superoxide dismutase (SOD; Unigene3085_All) and SOD[Cu-Zn] (Unigene6367_All) were upregulated in green to attenuate the deleterious effect of reactive oxygen species (ROS). Unigene4933_All, representing glutathione S-transferase (GST), was upregulated to exert antioxidant activities. Both GST and N-acetyltransferase (NAT) are phase II xenobiotic metabolizing enzymes (Hao et al. 2010). NAT enables acetyl coenzyme A-dependent detoxification of aromatic amines (Cocaign et al. 2013). Five Unigenes, representing NATs, were significantly upregulated in green as compared with ordi, one of which (Unigene622_All) clustered with laccase.

KEGG pathway enrichment analyses of DEGs. Significantly enriched metabolic pathways of DEGs after RG19 treatment were identified. After Bonferroni corrections of *p* values, eight, 14, and 24 KEGG pathways are still enriched in DEGs of ordi vs. green, ordi vs. guai and guai vs. green, respectively. "Biosynthesis of secondary metabolites" and "Metabolic pathways" were significantly enriched in all three comparisons (Fig. S3),

indicating the enhancement of secondary metabolite biosynthesis and the overall metabolism in response to the attack of azo dye/phenolic. In guai vs. green, the enrichment of "Ascorbate and aldarate metabolism" and "Nitrogen metabolism" suggests the increased antioxidant activity and enhanced nitrogen turnover during azo dye biodegradation and metabolism, respectively; "Carbon metabolism" and "MAPK signaling pathway" were also more active after azo dye stimulation. The changes in "Biosynthesis of antibiotics" are implicated as defense responses.

Enzyme activity. Transcriptome sequencing results suggest that both enzymes: oxidase, e.g., laccase, AAO, tyrosinase, peroxidase, and reductase including ferric reductase could be involved in biodegradation of azo dyes. Azo reductase and NADH-DCIP reductase were involved in reductive cleavage of azo bonds, which was the first step of biodegradation of azo compounds in some microbes (Solis et al. 2012; Song et al. 2017). Although the gene expression of these two reductases was not found to be upregulated in the transcriptome analysis, their activities, along with those of other six enzymes, were quantified. The activity of MnP was not detected intracellularly and extracellularly, which corresponded to the significant downregulation of MnP expression after RG19 treatment. On the contrary, LiP can be quantified intracellularly and extracellularly (Table I), and its activity was higher in the presence of RG19 when compared with no RG19, albeit the differences between two conditions were not statistically significant. Tyrosinase also showed the trend of higher activity in the presence of RG19 when compared with no RG19, regardless of intracellularly or extracellularly, but the differences between dye presence and dye absence were not statistically significant. In contrast, RG19 significantly induced the extracellular laccase activity (Table I); RG19 also substantially induced the intracellular and extracellular AAO activity. These data, taken together with transcriptome results, suggest the major role of laccase and AAO, and minor role of LiP and tyrosinase in decolorization and biotransformation of azo dye in *M. verrucaria* strain DJTU-sh7.

NADH-DCIP reductase was involved in cleavage of azo bonds (Song et al. 2017), which were the chromophoric groups of azo dyes. NADH-DCIP reductase was detected intracellularly and extracellularly in the presence or absence of RG19, and the extracellular enzyme activity was higher than the intracellular one. The differences of NADH-DCIP reductase activity were not statistically significant between RG19 treatment and no RG19 (Table I), so were the differences of azo reductase. These data suggest that the activity of both reductases was not induced by RG19. Rather, the activity of ferric reductase might be induced by RG19, as its intracellular and extracellular activity was significantly higher after RG19 exposure. This suggests its prominent role in decolorization and biotransformation of azo dye in *M. verrucaria*.

Conclusion and prospect

For the first time, laccase-producing fungi were isolated from *Taxus* rhizosphere. The statistically-based uniform design is well suited for optimizing the laccase-producing medium composition. *M. verrucaria* strain DJTU-sh7 proved to be most efficient in decolorizing nine reactive dyes at a broad range of pH and temperature, and the dye degradation was confirmed by chromatographic and spectral analyses. The good performance of DJTU-sh7-containing fungal consortium implies its utility in the treatment of industrial dye effluent.

The characterization of *M. verrucaria* DJTU-sh7 was strengthened by the mechanism views contributed by the transcriptome characterization of this dye-decolorizing strain. The gene expressions of multiple oxidases and reductases were significantly upregulated after azo

Table I
Enzyme activities of *M. verrucaria* strain DJTU-sh7 in decolorizing RG19.

Enzyme (U/ml)	RG19 addition		No RG19	
	Intracellular	Extracellular	Intracellular	Extracellular
Laccase	ND	26.241 ± 0.760*	ND	17.108 ± 0.895
Lignin peroxidase	0.164 ± 0.006^	0.120 ± 0.006^	0.152 ± 0.017	0.097 ± 0.002
Mn peroxidase	ND	ND	ND	ND
Tyrosinase	45.000 ± 3.000^	38.667 ± 8.386^	42.333 ± 6.429	33.667 ± 2.309
Aryl alcohol oxidase	14.093 ± 0.056*	5.900 ± 0.001*	5.244 ± 0.056	3.572 ± 0.056
Ferric reductase	7.845 ± 0.137**	11.788 ± 0.182*	6.849 ± 0.068	9.000 ± 0.182
Azo reductase	22.853 ± 0.544^	12.696 ± 0.670^	23.242 ± 0.155	12.204 ± 0.432
NADH-DCIP reductase	3.644 ± 1.547^	8.926 ± 0.696^	2.603 ± 1.610	7.550 ± 2.260

Values are mean ± SD; *$p < 0.001$, **$p < 0.01$, ^$p > 0.05$ in Student's t-test as compared with no RG19. ND, not detected.

dye exposure, and the metabolic pathways underwent dramatic remodeling and reprogramming. Enzyme activity quantification highlighted the potentially important roles of laccase, aryl alcohol oxidase, and ferric reductase in decolorization and degradation of azo dye, which ultimately lead to mineralization through TCA cycle. Although extracellular laccase might be a major factor in the decolorization of the studied dyes, genes implicated in transcriptome analysis of dye transformation call for further mechanism studies and the process optimization at the industrial scale.

Acknowledgments

This work is supported by Liaoning Postgraduate Education and Teaching Reform Project (2016) and Natural Science Fund of Liaoning province (2015020663 and 20180550190).

Conflict of interest

Authors do not report any financial or personal connections with other persons or organizations, which might negatively affect the contents of this publication and/or claim authorship rights to this publication.

Literature

Akpinar M, Urek RO. 2014. Extracellular ligninolytic enzymes production by *Pleurotus eryngii* on agroindustrial wastes. Prep Biochem Biotechnol. 44:772–781.

Baratto MC, Juarez-Moreno K, Pogni R, Basosi R, Vazquez-Duhalt R. 2015. EPR and LC-MS studies on the mechanism of industrial dye decolorization by versatile peroxidase from *Bjerkandera adusta*. Environ Sci Pollut Res Int. 22:8683–8692.

Bello-Gil D, Roig-Molina E, Fonseca J, Sarmiento-Ferrández MD, Ferrándiz M, Franco E, Mira E, Maestro B, Sanz JM. 2018. An enzymatic system for decolorization of wastewater dyes using immobilized CueO laccase-like multicopper oxidase on poly-3-hydroxybutyrate. Microb Biotechnol. 11(5):881–892.

Buchfink B, Xie C, Huson DH. 2015. Fast and sensitive protein alignment using DIAMOND. Nat Methods. 12:59–60.

Chitradevi V, Sivakumar V. 2011. Optimization and kinetics evaluation of biodegradation of synthetic azo reactive dye by fungal consortium. J Environ Sci Eng. 53:487–492.

Cirik K, Kitis M, Cinar O. 2013. The effect of biological sulfate reduction on anaerobic color removal in anaerobic-aerobic sequencing batch reactors. Bioprocess Biosyst Eng. 36:579–589.

Cocaign A, Bui LC, Silar P, Chan Ho Tong L. 2013. Biotransformation of *Trichoderma* spp. and their tolerance to aromatic amines, a major class of pollutants. Appl Environ Microbiol. 79:4719–4726.

Dawkar VV, Jadhav UU, Tamboli DP, Govindwar SP. 2010. Efficient industrial dye decolorization by *Bacillus* sp. VUS with its enzyme system. Ecotoxicol Environ Saf. 73:1696–1703.

Dou TY, Ge GB, Hao DC, Yang L. 2015. Functional and structural properties of a novel cellulosome-like multienzyme complex: efficient glycoside hydrolysis of water-insoluble 7-xylosyl-10-deacetylpaclitaxel. Sci Rep. 5:13768.

Ferreira P, Medina M, Guillén F, Martínez MJ. 2005. Spectral and catalytic properties of aryl-alcohol oxidase, a fungal flavoenzyme acting on polyunsaturated alcohols. Biochem J. 389:731–738.

Forootanfar H, Faramarzi MA. 2015. Insights into laccase producing organisms, fermentation states, purification strategies, and biotechnological applications. Biotechnol Prog. 31:1443–1463.

Gomaa OM, Selim NS, Wee J, Linz JE. 2017. RNA Seq analysis of the role of calcium chloride stress and electron transport in mitochondria for malachite green decolorization by *Aspergillus niger*. Fungal Genet Biol. 105:1–7.

Hao DC, Chen SL, Osbourn A, Liu LW. 2015. Temporal transcriptome changes induced by methyl jasmonate in *Salvia sclarea*. Gene 558:41–53.

Hao DC, Ge GB, Xiao PG, Zhang Y, Yang L. 2011. The first insight into the tissue specific taxus transcriptome via Illumina second generation sequencing. PLoS One 6:e21220.

Hao DC, Ge GB, Yang L. 2008. Bacterial diversity of *Taxus* rhizosphere: culture-independent and culture-dependent approaches. FEMS Microbiol Lett. 284:204–212.

Hao DC, Song SM, Mu J, Hu WL, Xiao PG. 2016. Unearthing microbial diversity of *Taxus* rhizosphere via MiSeq high-throughput amplicon sequencing and isolate characterization. Sci Rep. 6:22006.

Hao DC, Xiao PG. 2011. Prediction of sites under adaptive evolution in flavin-containing monooxygenases: Selection pattern revisited. Chin Sci Bull. 56:1246–1255.

Hao DC, Xiao PG, Chen SL. 2010. Phenotype prediction of non-synonymous single nucleotide polymorphisms in human phase II drug/xenobiotic metabolizing enzymes: perspectives on molecular evolution. Sci China Life Sci. 53:1252–1262.

Hong YG, Gu JD. 2010. Physiology and biochemistry of reduction of azo compounds by *Shewanella* strains relevant to electron transport chain. Appl Microbiol Biotechnol. 88:637–643.

Hsueh CC, Chen BY, Yen CY. 2009. Understanding effects of chemical structure on azo dye decolorization characteristics by *Aeromonas hydrophila*. J Hazard Mater. 167:995–1001.

Jasińska A, Paraszkiewicz K, Sip A, Długoński J. 2015. Malachite green decolorization by the filamentous fungus *Myrothecium roridum* – Mechanistic study and process optimization. Bioresour Technol. 194:43–48.

Khan R, Fulekar MH. 2017. Mineralization of a sulfonated textile dye Reactive Red 31 from simulated wastewater using pellets of *Aspergillus bombycis*. Bioresour Bioprocess. 4:23.

Khandare RV, Rane NR, Waghmode TR, Govindwar SP. 2012. Bacterial assisted phytoremediation for enhanced degradation of highly sulfonateddiazo reactive dye. Environ. Sci Pollut Res Int. 19:1709–1718.

Kim SJ, Kweon O, Jones RC, Freeman JP. 2007. Complete and integrated pyrene degradation pathway in *Mycobacterium vanbaalenii* PYR-1 based on systems biology. J Bacteriol. 189:464–472.

Klema VJ, Solheid CJ, Klinman JP, Wilmot CM. 2013. Structural analysis of aliphatic versus aromatic substrate specificity in a copper amine oxidase from *Hansenula polymorpha*. Biochemistry 52: 2291–2301.

Kumar L, E Futschik M. 2007. Mfuzz: a software package for soft clustering of microarray data. Bioinformation 2:5–7.

Kumari K, Abraham TE. 2007. Biosorption of anionic textile dyes by nonviable biomass of fungi and yeast. Bioresour Technol. 98: 1704–1710.

Ma HY, Ning J, Ge GB, Yang L, Hao DC. 2017. Research progress of human cytochrome P450 2J2 and its ligands. Acta Pharm Sin. 52:26–33.

Ng IS, Xu F, Ye C, Chen BY, Lu Y. 2014. Exploring metal effects and synergistic interactions of ferric stimulation on azo-dye decolorization by new indigenous *Acinetobacter guillouiae* Ax-9 and *Rahnella aquatilis* DX2b. Bioprocess Biosyst Eng. 37:217–224.

Nor NM, Hadibarata T, Zubir MM, Lazim ZM. 2015. Mechanism of triphenylmethane Cresol Red degradation by *Trichoderma harzianum* M06. Bioprocess Biosyst Eng. 38:2167–2175.

Patel TL, Patel BC, Kadam AA, Tipre DR, Dave SR. 2015. Application of novel consortium TSR for treatment of industrial dye manu-

facturing effluent with concurrent removal of ADMI, COD, heavy metals and toxicity. Water Sci Technol. 71:1293–1300.

Ramalho PA, Paiva S, Cavaco-Paulo A, Casal M. 2005. Azo reductase activity of intact saccharomyces cerevisiae cells is dependent on the Fre1p component of plasma membrane ferric reductase. Appl Environ Microbiol. 71:3882–3888.

Rodríguez-Sáiz M, Barredo JL, Moreno MA, Fernández-Cañón JM. 2001. Reduced function of a phenylacetate-oxidizing cytochrome p450 caused strong genetic improvement in early phylogeny of penicillin-producing strains. J Bacteriol. 183: 465–5471.

Schaechter M. 2009. Encyclopedia of microbiology (Third edition). London (UK): Academic Press.

Sheikhi F, M Roayaei Ardakani, N. Enayatizamir and S. Rodriguez-Couto. 2012. The determination of assay for laccase of *Bacillus subtilis* WPI with two classes of chemical compounds as substrates. Indian J Microbiol. 52:701–707.

Shimokawa T, Hirai M, Shoda M, Sugano Y. 2008. Efficient dye decolorization and production of dye decolorizing enzymes by the basidiomycete *Thanatephorus cucumeris* Dec 1 in a liquid and solid hybrid culture. J Biosci Bioeng. 106:481–487.

Solis M, Solis A, Perez HI, Manjarrez N, Flores M. 2012. Microbial decolouration of azo dyes: A review. Process Biochem. 47:1723–1748.

Song L, Shao Y, Ning S, Tan L. 2017. Performance of a newly isolated salt-tolerant yeast strain *Pichia occidentalis* G1 for degrading and detoxifying azo dyes. Bioresour Technol. 233:21–29.

Sun J, Jin J, Beger RD, Cerniglia CE, Chen H. 2017. Evaluation of metabolism of azo dyes and their effects on *Staphylococcus aureus* metabolome. J Ind Microbiol Biotechnol. 44:1471–1481.

Sun S, Xie S, Chen H, Cheng Y. 2016. Genomic and molecular mechanisms for efficient biodegradation of aromatic dye. J Hazard Mater. 302:286–295.

Waghmode TR, Kuradeb MB, Govindwar SP. 2011. Time dependent degradation of mixture of structurally different azo and non azo dyes by using *Galactomyces geotrichum* MTCC 1360. Int Biodeteri Biodegra. 65:479–486.

Xu M, Guo J, Kong X, Chen X, Sun G. 2007. Fe(III)-enhanced azo reduction by *Shewanella decoloration* is S12. Appl Microbiol Biotechnol. 74:1342–1349.

Xu N, Qian K, Dong Y, Chen Y. 2014. Novel role of the *Candida albicans* ferric reductase gene CFL1 in iron acquisition, oxidative stress tolerance, morphogenesis and virulence. Res Microbiol. 165:252–261.

Yu Q, Dong Y, Xu N, Qian K. 2014. A novel role of the ferric reductase Cfl1 in cell wall integrity, mitochondrial function, and invasion to host cells in *Candida albicans*. FEMS Yeast Res. 14:1037–1047.

Zhan X, Carpenter RA, Ellis HR. 2008. Catalytic importance of the substrate binding order for the $FMNH_2$-dependent alkanesulfonate monooxygenase enzyme. Biochemistry 47:2221–2230.

Zhao D, Zhang X, Cui D, Zhao M. 2012. Characterisation of a novel white laccase from the deuteromycete fungus *Myrothecium verrucaria* NF-05 and its decolourisation of dyes. PLoS One 7:e38817.

Supplementary materials are available on the journal's website.